Ultrasonic Periodontal Probing Based on the Dynamic Wavelet Fingerprint

Jidong Hou, S. Timothy Rose and Mark K. Hinders

Manual pocket depth probing has been widely used as a retrospective diagnosis method in periodontics. However, numerous studies have questioned its ability to accurately measure the anatomic pocket depth. In this paper, an ultrasonic periodontal probing method is described, which involves using a hollow water-filled probe to focus a narrow beam of ultrasound energy into and out of the periodontal pocket, followed by automatic processing of pulse-echo signals to obtain the periodontal pocket depth. The signal processing algorithm consists of three steps: peak detection/characterization, peak classification and peak identification. A dynamic wavelet fingerprint (DWFP) technique was first applied to detect suspected scatterers in the A-scan signal and generate a two-dimensional black and white pattern to characterize the local transient signal corresponding to each scatterer. These DWFP patterns were then classified by a two-dimensional FFT procedure and mapped to an inclination index curve. The location of the pocket bottom was identified as the third broad peak in the inclination index curve. The algorithm was tested on full mouth probing data from two sequential visits of 14 patients. Its performance was evaluated by comparing ultrasonic probing results with that of full-mouth manual probing at the same sites, which was taken as the 'gold standard'.

I. INTRODUCTION

Most adults have a mild form of periodontal disease, while over 20 percent of older Americans have severe periodontal disease.[1,2,3] Periodontal disease involves the loss of tooth connective tissue (attachment) with subsequent destruction of tooth-supporting bone, leading to loss of teeth. In addition to being a major cause of tooth loss, periodontal disease has recently been associated with several systemic diseases. Animal and population-based studies have demonstrated an association between periodontal disease and diabetes, cardiovascular disease, stroke, and adverse pregnancy outcomes.[4,5,6] Despite the widespread problem of periodontal disease today, currently available diagnostic tests are limited in their effectiveness. None are a completely reliable indicator of periodontal disease activity and the best available diagnostic aid, probing pocket depths, is only a retrospective analysis of attachment already lost.[7-13] In traditional probing, which is now routinely done in the general dentistry office,[14] a metal probe is inserted between the soft tissue of the gingival margin (gum line) and the tooth. Using fixed markings on the probe, the depth of probe penetration is typically measured relative to the gingival margin.

Numerous studies have questioned the ability of the periodontal probe to accurately measure the anatomic pocket depth.[15-18] The degree of probe tip penetration may be influenced by factors such as thickness of the probe, pressure applied, tooth contour, tooth position, presence of calculus, degree of periodontal inflammation, and the actual level of connective tissue fibers.[19-24] As a result, probing measurements may

Keywords: ultrasonic, periodontal, probe, wavelet

Jidong Hou is with the Department of Applied Science, College of William and Mary, Williamsburg, VA 23187.

S. Timothy Rose, DDS is with Valley Periodontics, 2535 Northern Road, Appleton, WI 54914.

Mark K Hinders, PhD is with the Department of Applied Science, College of William and Mary, Williamsburg, VA 23187-8795 (telephone: 757-221-1519, e-mail: hinders@ as.wm.edu). (Contact author).

overestimate attachment loss by as much as 2 mm in untreated sites, while underestimating attachment loss by an even greater margin following treatment.[25,26] The development of automated, controlled-force probes has reduced some of the operator-related error and subjectivity inherent in manual probing techniques.[27-30] However, standardized probing forces do not address anatomic and inflammatory factors.[31-32]

The first tests of ultrasonic imaging of the periodontal space attempted to image the crest of the aveolar bone by aiming the ultrasound transducer perpendicular to the long axis of the tooth.[33-35] While these efforts proved the feasibility of ultrasonic imaging in dentistry, this version of the technique could not detect periodontal attachment loss, and failed to gain clinical acceptance. Recently, researchers have begun exploring new uses of ultrasound in dentistry[36-39] and studies have been conducted using ultrasound to image the periodontal pocket space by aiming the transducer *apically* into the pocket from the gingival margin.[40-46] The major technical barrier to this approach is providing an efficient coupling medium for the ultrasonic wave into the thin (0.25 - 0.5 mm) periodontal pocket. The probe described by Hinders and Companion uses a slight flow of water to couple the ultrasound wave into the pocket space. A hollow tip placed over the transducer narrows the ultrasonic beam, so that the beam is approximately the same width as the opening into the sulcus at the gingival margin.

The ultrasonic probe works by projecting a narrow, high-frequency (10-15 MHz) ultrasonic pulse into the gingival sulcus/periodontal pocket, and then detecting echoes of the returning wave. The time series return signal (A-scan) can then be converted into a depth measurement by multiplying the time of arrival of the return signal by the speed of sound in water (1500 m/s) and dividing by two (since the signal travels into the pocket and back). Ultrasonic probing is entirely painless, is as fast as manual probing, and has the potential to yield much more diagnostic information by providing the dentist and patient with a graphical representation of changes in pocket depth. However, due to the inherent complexity in the way ultrasonic waves interact with the inner structure of periodontal anatomy, it is unrealistic to train a dental hygienist to read out the pocket depth by watching and interpreting the echo waveform. Automated interpretation of these echoes is what enables a practical clinical system.

As an initial effort to automate interpretation of the echoes, a time domain procedure was developed to simplify the waveforms and infer the depth of the periodontal pocket.[44-46] This procedure used a slope-detection algorithm to pick peaks in the A-Scan signal, followed by smoothing and averaging operations to eliminate small random variations. The pocket depth was then inferred by dividing the simplified waveform into three regions and assuming the second transition from weaker peaks to noise is the estimation of the bottom of the periodontal pocket. Unfortunately, in many cases it was difficult or even impossible to define such three distinctive regions based on the echo amplitude. Even if the second transition point can be called out in some way, the depth of the periodontal pocket can only be inferred from it approximately. To overcome these limitations, information other than echo amplitude should be used to develop sensitive and reliable models to estimate the bottom of the periodontal pocket.

The wavelet transform (WT) can be constructed as a bank of matched filters if the mother wavelet is chosen to be an efficient representation of the input signal itself, so it has been widely used to solve detection/estimation problems.[47-51] As a multi-resolution analysis approach, the WT is also an effective method to extract significant information from dynamic signals, which is often the key in automated signal classification applications.[52-56] To take advantage of this potential of the WT, a dynamic wavelet fingerprint technique[57] was adapted to develop a signal processing algorithm for the ultrasonic periodontal probe. In this approach, potential scatterers are first detected by picking peaks in the scale averaged power (SAP) curve. A two-dimensional black and white pattern, called a DWFP, is then generated at each peak location to characterize the local transient signal. A two-dimensional FFT procedure is then applied to generate an

inclination index for each DWFP pattern. The bottom of the periodontal pocket is then estimated from the third broad peak of the inclination index curve.

This paper is organized as follows. In Section II, the experimental device and procedure are described. The algorithm used in this work is discussed in Section III. The results are presented in Section IV. A discussion and conclusion is given in Section V.

II. Clinical Instrument And signals

The ultrasonic periodontal probe shown in Fig.1 was operated using a portable computer system. The probe itself included a 10 MHz piezo-composite transducer with a 2 mm-diameter active area. The transducer was housed within a contra-angled handpiece at the base of a hollow conical tip. The tip was designed to narrow the ultrasonic beam profile to 0.5 mm and to provide an area for water to sustain the ultrasonic wave and carry it into the periodontal pocket.

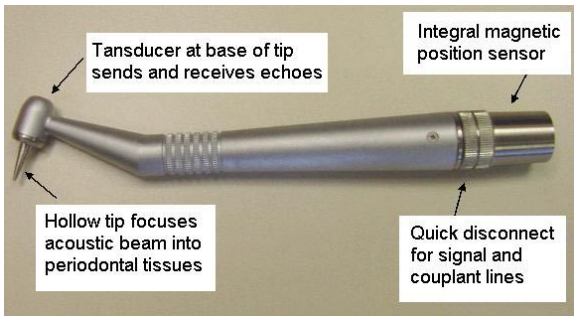

Fig.1 The ultrasonic probe handpiece.

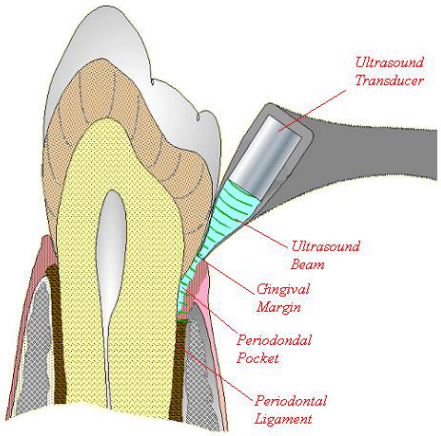

Fig.2 Schematic of ultrasonic periodontal probing.

Fig.2 illustrates how the ultrasonic probe is used to explore the periodontal pocket. A stream of water is used as couplant to launch ultrasound energy into the periodontal pocket. The ultrasound wave interacts with the periodontal tissue and echoes relevant information back to the transducer. During operation, the ultrasonic probe is held in a pose similar to manual probing but with its tip touching the gingival margin. The ultrasonic probe was held in place, momentarily at each of the standard probing locations to acquire a series of ultrasonic A-scan signals that were digitized and saved in the computer for later analysis. Water flow and data acquisition was automated via foot pedal control.

At Valley Periodontics, Appleton, WI, 14 patients were examined both by hand and by the ultrasonic instrument on two visits scheduled three months apart. For each patient, full mouth probing was carried out, first by hand and then by the ultrasonic instrument. For each of up to 32 teeth for each patient, a periodontist performed probing at 6 sites (facial distal, facial middle, facial mesial, lingual distal, lingual middle and lingual mesial), providing up to 192 corresponding ultrasonic and manual probing measurements per patient.

A typical A-scan signal obtained is shown in Fig.3 (a). The horizontal axis represents the time from 0 to 20.48 μs at 100MHz sampling rate. The vertical axis represents normalized voltage on an arbitrary scale digitized at 12 bits. The strong reflection region before point 2.5 μs arises from the echoes internal to the probe tip. After point 2.5 μs, it is the signal from the periodontal anatomy.

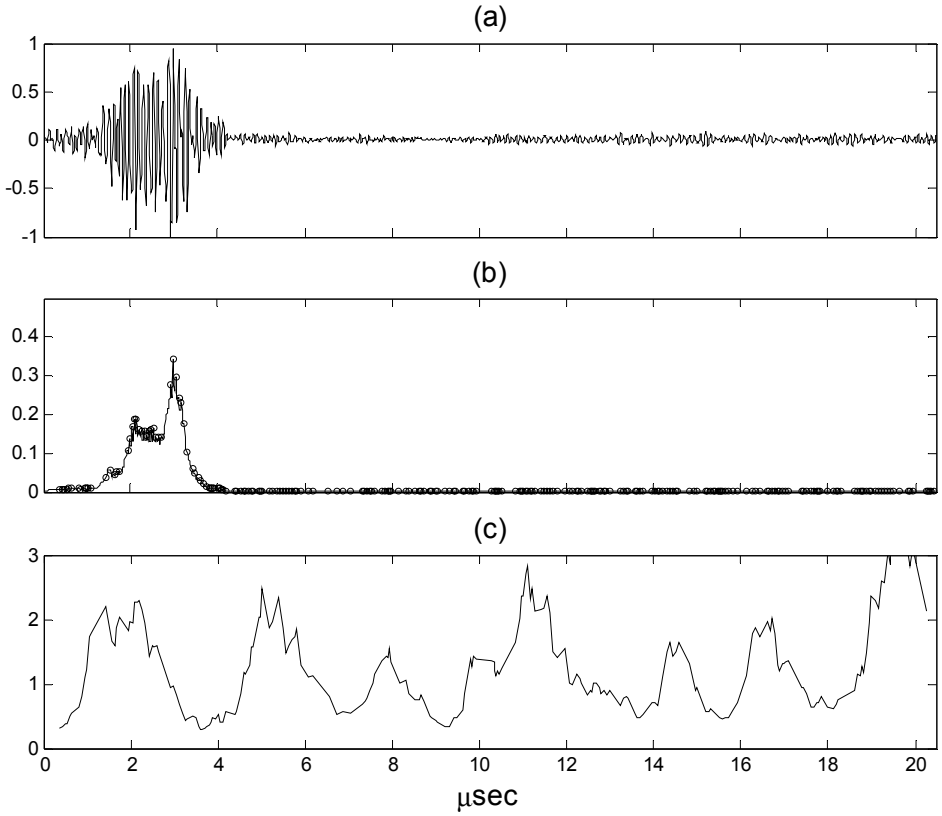

Fig.3. Illustration of signal processing for ultrasonic periodontal probing. (a) Original A-scan signal, (b) SAP peaks marked by the small circles, (c) The inclination index curve. The third significant peak (at about 8 μs) corresponds to the estimated location of the bottom of the periodontal pocket.

III. ALGORITHM DEVELOPMENT

A flowchart of the proposed algorithm is shown in Fig.4, which involves three main steps: peak detection/characterization, peak classification, and peak identification.

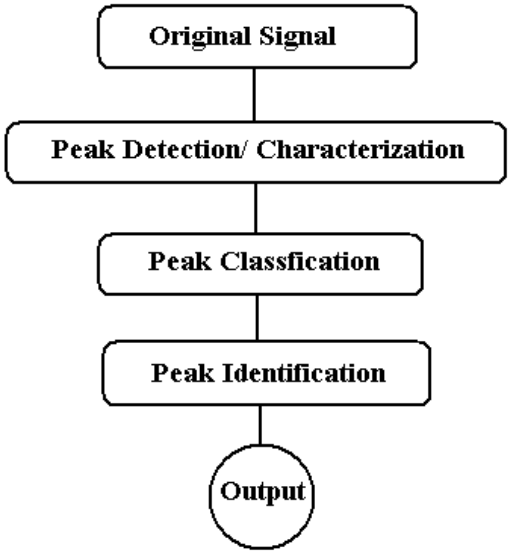

Fig.4. Flowchart of the algorithm used to process ultrasound signal to detect the bottom of the periodontal pocket.

A so-called dynamic wavelet fingerprint (DWFP) technique was recently introduced by two of the authors. It consists of peak detection operation followed by peak characterization.[57] The basic idea is to generate a simplified and intuitive two-dimensional pattern in time-scale domain for each detected transient signal, so that significant features can be extracted directly by watching the patterns or by using modern pattern recognition technique. These features then can be used to identify specific signal of interest. The proposed algorithm is explained as follows:

First, the scale-averaged wavelet power (SAP) proposed by Georgiou and Cohen[52] was calculated, i.e.,

$$W_a^2(n) = \frac{1}{J}\sum_{j=1}^{J} |W(s_j, n)|^2 \qquad (1)$$

where $W(s_j, n)$ is the continuous wavelet coefficients at scale s_j and position *n*, i.e.,

$$W(s_j, n) = \int_R f(t) \frac{1}{\sqrt{s_j}} \overline{\Psi(\frac{t-n}{s_j})}\, dt \qquad (2)$$

The results obtained by (1) were smoothed by a median filter to generate a SAP curve. SAP peaks were then picked out wherever the sign of the first derivative of the SAP curve changes from positive to negative as shown in Fig. 3(b). According to Georgiou and Cohen, the significant SAP peaks correspond to coherent scatterers that can be differentiated from the diffuse background. Assuming that the bottom of the periodontal pocket belongs to such coherent and resolvable scatterers, and that it can be detected as one of the SAP peaks, the question now is how to differentiate it from other scatterers.

To suppress noise and high frequency interference that may cause distortion of the DWFP pattern generated later, a pruning procedure[58] based on the stationary wavelet transform[59] was applied on the original A-scan signal, i.e.,

$$W_S(a,b) = 0 \quad for\ a = 1...5 \qquad (3)$$

where $W_S(a,b)$ is the stationary wavelet coefficients at scale *a* and time *b*.

Next, a continuous wavelet transform was performed on the pruned A-scan signal using the Morlet

wavelet[60-61]:

$$\psi(x) = Ce^{-x^2/2}\cos(5x)$$

where the constant C is used for normalization. Different choices for the mother wavelet will, of course, give different DWFPs[57] with some better highlighting features of interest in the signals under study than others. For the ultrasonic periodontal probing data the Morlet wavelet seemed to give DWFP sequences dominated by "loop" features with varying inclination, which could then be quantified in an automatic way.

For each peak in the SAP curve, the wavelet coefficients in its neighborhood are normalized into the range of [-1, +1] and then projected onto the time-scale plane to generate a two dimensional black and white pattern[57]. A typical DWFP sequence obtained is shown in Fig.5. In each frame of the sequence, time is the horizontal axis and wavelet scale is the vertical axis. This gives an abstract 2D representation which allows "patterns" in the data to be recognized even when none are evident in the 1D waveforms.

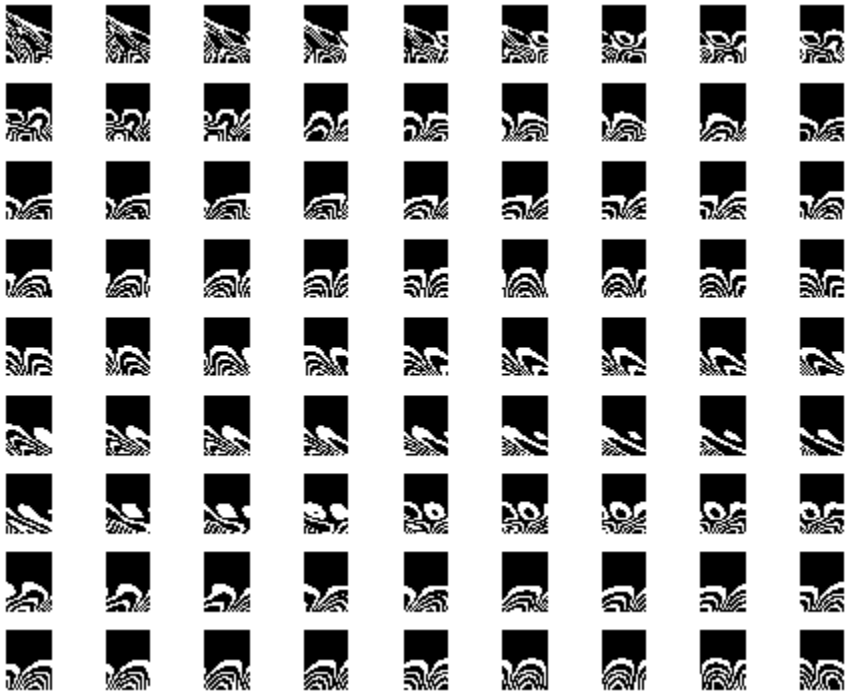

Fig.5. Typical DWFP sequence of an A-scan signal (time sequence: from left to right, from top to bottom).

By observing the DWFP sequences carefully, it was noted that these DWFP patterns change their inclination regularly, i.e., from left inclined to up-right and to right inclined, and repeating. A two-dimensional FFT based approach was designed to quantitatively characterize such variations.

Fig.6 shows three typical DWFP patterns from such a sequence along with their corresponding 2D FFT images. For the right inclined DWFP, it can be seen that its image is left diagonally dominated, i.e., there are more bright pixels at the top-left and bottom-right corners than at the top-right and bottom-left corners. On the contrary, for the left inclined DWFP, its image is right diagonally dominated. For the up-right DWFP, its two-dimensional FFT image is almost symmetric.

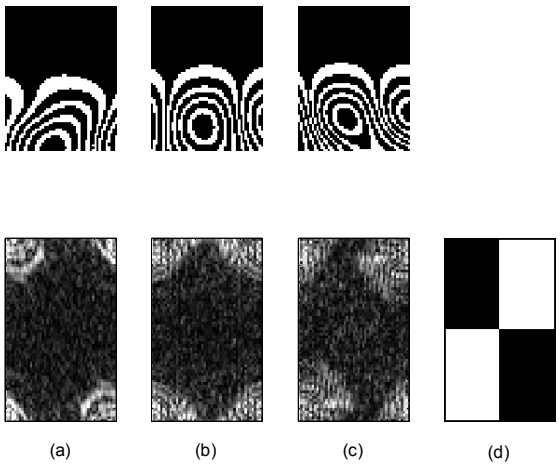

Fig.6. Two-dimensional FFT images of three typical DWFP patterns. (a) Right inclined DWFP (b) Up-right DWFP (c) Left inclined DWFP (d) Two regions used to calculate the inclination index of the two-dimensional FFT image.

Based on these observations, each two-dimensional FFT image was divided into two pairs of quadrants as shown in Fig.6(d). An inclination index, *Ix*, was defined as the ratio of the number of white pixels in the shaded quadrants to that in the unshaded quadrants. The DWFP sequence was then mapped into an *Ix* curve as shown in Fig.3(c). The regular variation of the DWFP is thus displayed as identifiable peaks and valleys.

To better explore the relationship between this intuitive pattern variation and the complex physics behind it, the same system was used to probe a simplified phantom built in a block of steel with holes of different depth (Fig. 7). This sort of is typically used to calibrate new automatic periodontal probes, and although it doesn't represent all of the complicated periodontal pocket anatomy it does provide us with an ultrasonically well-characterized system with which we can be certain that our algorithms are isolating true ultrasonic echoes from noise/artifacts inherent in the probing measurement.

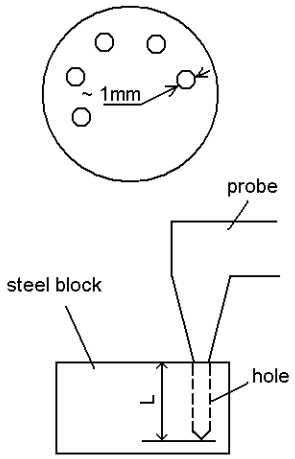

Fig.7. Phantom probing using the ultrasonic probe.

Fig.8 illustrates an A-scan signal and its corresponding processing results. In the *Ix* curve, similar peaks and valleys can be seen as in Fig.3(c). It is clear that the first significant peak corresponds to the reflection from the probe tip at about point 2.5 μs, and the third significant peak is closed to the reflection from the bottom of the hole. As for the second significant peak in between, it is assumed be caused by the interference of the water flow and the reflections of the wall of the hole. Accordingly, a qualitative explanation was proposed

to describe the regular peaks and valleys in the *Ix* curve of the ultrasonic periodontal probing signal: the first significant peak arises from the probe tip, the second significant peak may be caused by the tooth surface, and the third significant peak may correspond to the bottom of the periodontal pocket. After the location of the bottom of the periodontal pocket is estimated as above, the pocket depth is calculated as the product of the time delay from the probe tip and the speed of ultrasound in water (1.5mm/ μs), then divided by two.

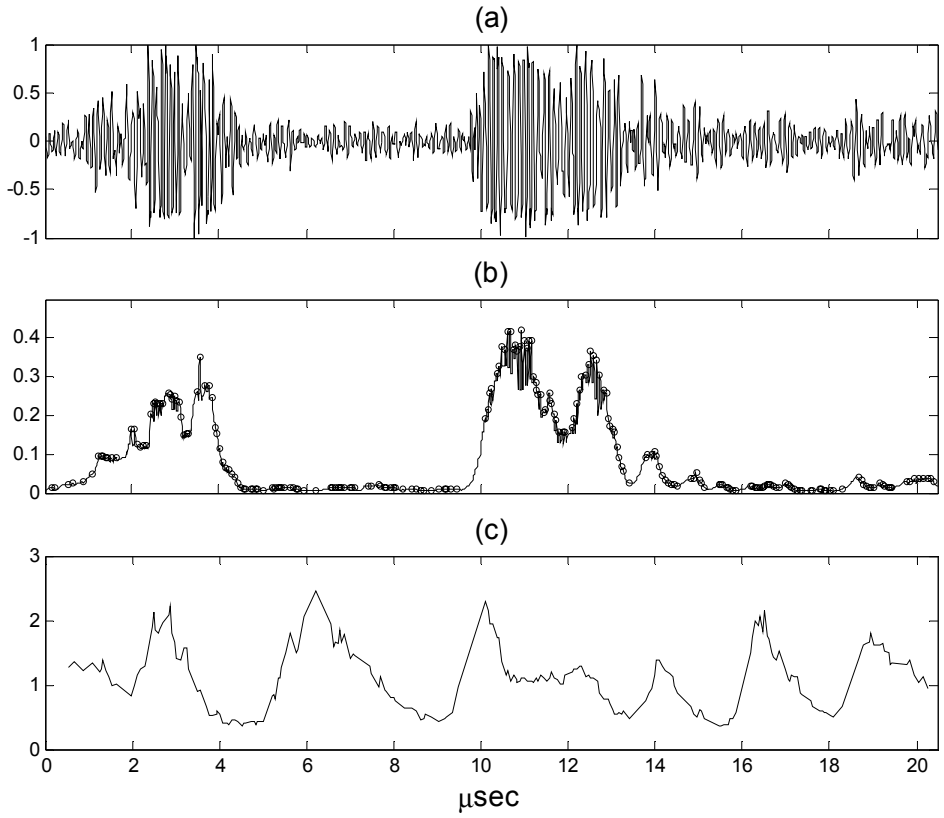

Fig.8. Phantom probing signal and corresponding processing results. (a) Original A-scan signal, (b) SAP peaks (c) the inclination index curve. The third broad peak corresponds to the reflection from the bottom of the hole.

IV. RESULTS

A MatLab (The MathWorks, Inc) program was developed to process full mouth ultrasonic probing data of 14 patients acquired during two clinical sessions. It works in off-line mode and runs automatically until all of the digitized A-scan signals are processed.

Because of the lack of any ideal standard to compare with, we take the manual probing result as the "gold standard" and compare it with ultrasonic probing, keeping in mind that an accuracy of ± 1 mm for manual probing is perhaps being generous.

Firstly, ultrasonic probing readings were compared with manual probing readings at each probing site. If we allow for the "error bar" of ± 0.5 mm, ± 1.0 mm and ± 1.5 mm respectively, the agreement ratio (number of ultrasonic probing measurements within the "error bar" divided by number of total ultrasonic probing results) is about 20%, 40% and 60% correspondingly as shown in Fig.9.

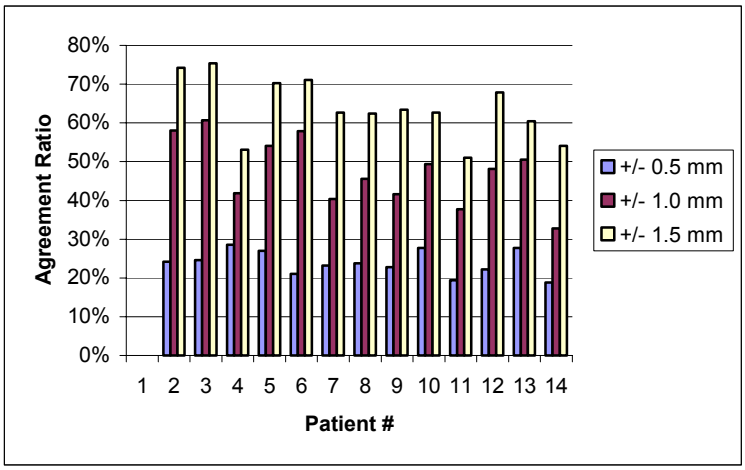

(a)

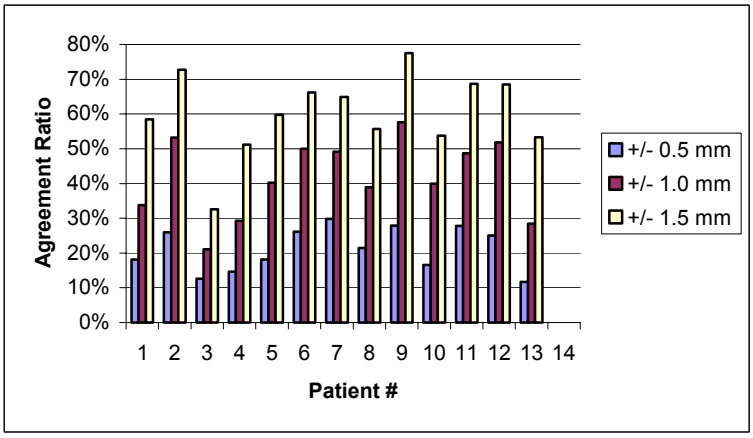

(b)

Fig.9. Ratio of agreement of ultrasonic probing vs. manual probing. (a) May 18, 2001 (b) August 17, 2001. Note that results for patient #1 in (a) and patient #14 in (b) are unavailable due to personal absence in corresponding clinical visit.

Statistically, the agreement between ultrasonic probing and manual probing was evaluated by the Bland-Altman method[62].

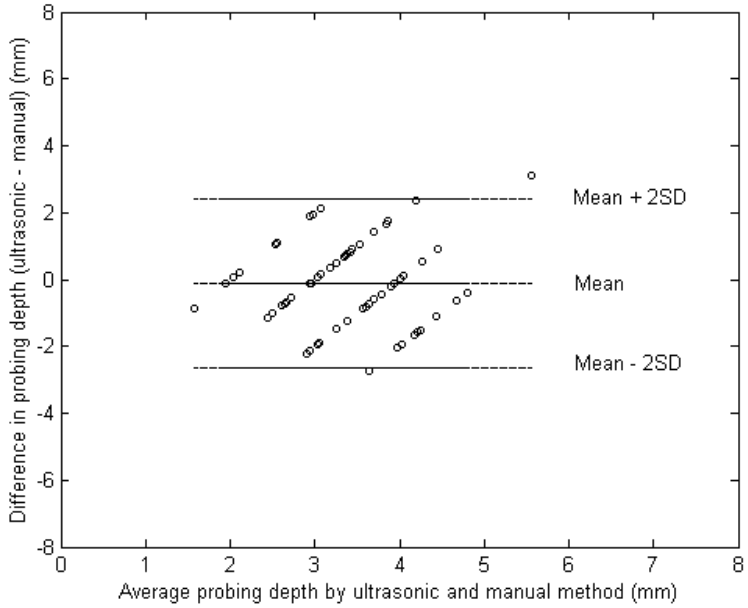

Fig.10. Difference against mean for periodontal probing depth of Patient #2, May 18.

As an example, a plot of the difference between the methods and their mean was drawn for patient #2, May 18, in Figure 10. It seems that the difference does not increase with the mean. The regular gaps are due to integer measurements of manual probing. Assume the difference is normally distributed, the mean difference $\overline{d}$ and the standard deviation SD of the difference was calculated as $\overline{d} = -0.1128$ and SD =1.2611. The "limits of agreement" can be obtained as:

$$\overline{d} - 2SD = -0.1128 - (2 \times 1.2611) = -2.635 \text{ mm}$$

$$\overline{d} + 2SD = -0.1128 + (2 \times 1.2611) = 2.409 \text{ mm}$$

According to Bland and Altman, about 95% of differences will lie between these limits. In other words, the ultrasonic probing depth may be 2.6 mm below or 2.4 mm above the manual probing depth. The precision of the estimation of $\overline{d}$, $\overline{d} + 2SD$ and $\overline{d} - 2SD$ can be evaluated by using 95% confidence interval of a *t*-distribution with n-1 degree of freedom, where n is the sample size. For the patient chosen above, these confidence intervals were obtained as [-0.3818 0.1563], [1.9433 2.8754] and [-3.1010 -2.1689], repectively. Similar calculations were performed on other data sets and the results were presented in Tables 1 and 2.

Taking the non-zero $\overline{d}$ into consideration, the "limits of agreement" are generally in the range of ± 3mm. This may indicate a lack of agreement between ultrasonic probing and manaul probing, which could be caused by several factors. The specific anatomical features measured by the two methods may be different; the probing point and angle may not be exactly same. More likely, it may arise from the model used in the algorithm. As mentioned above, the regular variation of the inclination of the DWFP patterns is motivated by an experiment on a steel block phantom, which is not entirely representative of the problem at hand, even though it does eliminate the sizeable error in the manual probing "gold standard." To better understand the regular variation of the DWFP patterns, a more accurate model should be developed guided by systematic clinical experiments carried out in the future.

TABLE 1

a. Mean Difference $\bar{d}$ and Its 95% Confidence Intervals (May 18)

Patient #	1	2	3	4	5	6	7	8	9	10	11	12	13	14
$\bar{d}$	N/A	-0.1128	0.4532	0.1722	0.8217	0.0176	-0.7202	0.2462	0.1853	-0.7140	-0.3904	-0.0353	-0.6021	-1.2224
Low Limit	N/A	-0.3818	0.1741	-0.1305	0.5303	-0.3553	-1.0045	-0.0501	-0.0714	-0.9960	-0.7110	-0.3243	-0.8485	-1.4429
High Limit	N/A	0.1563	0.7323	0.4750	1.1130	0.3905	-0.4360	0.5425	0.4421	-0.4320	-0.0697	0.2538	-0.3557	-1.0019

b. Limits of agreement $\bar{d} \pm 2SD$ and their 95% Confidence Intervals (May 18)

Patient #	1	2	3	4	5	6	7	8	9	10	11	12	13	14
$\bar{d} + 2SD$	N/A	2.4094	3.0481	3.7399	3.8056	2.7541	2.6465	3.7914	3.2574	2.3447	3.3886	3.0618	2.3459	1.6769
Low Limit	N/A	1.9433	2.5647	3.2156	3.3009	2.1082	2.1542	3.2782	2.8127	1.8562	2.8332	2.5612	1.9191	1.2950
High Limit	N/A	2.8754	3.5315	4.2643	4.3103	3.3999	3.1388	4.3047	3.7021	2.8331	3.9440	3.5625	2.7727	2.0588
$\bar{d} - 2SD$	N/A	-2.6349	-2.1417	-3.3955	-2.1623	-2.7188	-4.0869	-3.2991	-2.8867	-3.7726	-4.1693	-3.1324	-3.5502	-4.1217
Low Limit	N/A	-3.1010	-2.6251	-3.9199	-2.6669	-3.3647	-4.5792	-3.8123	-3.3315	-4.2611	-4.7247	-3.6331	-3.9769	-4.5036
High Limit	N/A	-2.1689	-1.6583	-2.8712	-1.6576	-2.0729	-3.5946	-2.7858	-2.4420	-3.2842	-3.6139	-2.6317	-3.1234	-3.7398

N/A- patient not available

TABLE 2

a. Mean Difference $\bar{d}$ and Its 95% Confidence Intervals (August 17)

Patient #	1	2	3	4	5	6	7	8	9	10	11	12	13	14
$\bar{d}$	-0.0383	0.4431	2.1375	0.0154	-0.7111	0.4561	0.1884	0.9767	0.5739	1.2619	-0.0827	0.1696	1.3116	N/A
Low Limit	-0.3708	0.2035	1.9106	-0.5105	-1.0207	0.2277	-0.0732	0.7546	0.3573	1.0374	-0.3309	-0.0641	1.0875	N/A
High Limit	0.2941	0.6826	2.3644	0.5414	-0.4015	0.6844	0.4500	1.1989	0.7905	1.4863	0.1654	0.4034	1.5356	N/A

b. Limits of agreement $\bar{d} \pm 2SD$ and their 95% Confidence Intervals (August 17)

Patient #	1	2	3	4	5	6	7	8	9	10	11	12	13	14
$\bar{d} + 2SD$	3.4348	2.9452	4.7704	4.0246	2.5230	3.5555	3.5133	4.2047	3.2903	4.4792	3.0848	3.0615	4.4338	N/A
Low Limit	2.8589	2.5303	4.3774	3.1137	1.9868	3.1600	3.0602	3.8200	2.9152	4.0904	2.6551	2.6567	4.0457	N/A
High Limit	4.0106	3.3601	5.1634	4.9356	3.0592	3.9510	3.9664	4.5895	3.6655	4.8679	3.5146	3.4664	4.8219	N/A
$\bar{d} - 2SD$	-3.5115	-2.0591	-0.4953	-3.9938	-3.9452	-2.6434	-3.1365	-2.2513	-2.1425	-1.9554	-3.2503	-2.7223	-1.8107	N/A
Low Limit	-4.0873	-2.4739	-0.8884	-4.9048	-4.4814	-3.0389	-3.5895	-2.6360	-2.5176	-2.3441	-3.6801	-3.1271	-2.1988	N/A
High Limit	-2.9356	-1.6442	-0.1023	-3.0828	-3.4089	-2.2479	-2.6834	-1.8665	-1.7674	-1.5667	-2.8206	-2.3174	-1.4226	N/A

N/A- patient not available

V. Conclusion

An ultrasonic periodontal probing instrument is being developed. It uses a hollow water-filled tip to couple the ultrasound energy into and back out of the periodontal pocket, thus probing the periodontal anatomy by a non-invasive, painless and automatic technique. Key to automation of the probing is an ultrasonic signal processing algorithm for the periodontal probing instrument, which uses a dynamic wavelet fingerprint technique to detect and characterize the transient signals arise from each suspected scatterer and estimate the location of the echoes corresponding to the bottom of the periodontal pocket.

Clinical data from 14 patients have been processed with the proposed algorithm. Site by site comparison shows about 40% agreement ratio between ultrasonic and manual probing at the tolerance of ±1.0 mm. Statistically, however, lack of agreement between ultrasonic and manual probing was found in terms of the "limits of agreement" proposed by Bland and Altman. It may arise from the model used in the algorithm and further research is necessary to develop more accurate phantom and understand the physics behind the intuitive variation of the DWFP patterns.

Acknowledgments

The authors would like to thank Jonathan Stevens for constructing much of the instrumentation and the new handpiece. This work was supported by the National Institute of Dental and Craniofacial Research (No. 1R15DE12851-01 and No. 1R43DE1255701-A2) and by Virginia's Center for Innovative Technology (No. BIO-01-004).

References

[1] Evans, C.A., Leinman D.V., Maas, W.R., et al. *Oral Health in America: A Report to the Surgeon General.* (Bethesda, Maryland: National Institute of Dental and Craniofacial Research. 2000). NIH publication no. 00-4713.

[2] Barrington, E.P. and Nevins, M., Diagnosing periodontal diseases. *J. Am. Dental Assoc 121*, 460-464, (1990).

[3] Armitage, G.C. et al. Diagnosis of Periodontal Diseases, Academy Report Position Paper. *J. Periodontol. 74,* 1237-1247, (2003).

[4] Fowler, E.B., Periodontal disease and its association with systemic disease. *Military Medicine 166,* 85-89, (2001).

[5] Paquette, D.W., The periodontal infection-systemic disease link: a review of the truth or myth. *J. Int. Acad. of Periodontology 4,* 101-109 (2002).

[6] Slots, J. Update on general health risk of periodontal disease. *International Dental Journal* 53, 200-207 (2003).

[7] Haffajee, A.D., et al., Clinical parameters as predictors of destructive periodontal disease activity. *J. Clinical Periodontology 10,* 257, (1982).

[8] Tessier, J.F., et al. Probing velocity: novel approach for assessment of inflamed periodontal attachment. *J. Periodontology 65,* 103-108 (1994).

[9] Hull, P.S., Clerehugh, V., and Ghassemi-Aval, A., An assessment of the validity of a constant force electronic probe in measuring probing depths. *J. Periodontology 66,* 848-851, (1995).

[10] Rams, T.E. and Slots, J., Comparison of two pressure-sensitive periodontal probes and a manual probe in shallow and deep pockets. *Int. J. of Periodontics & Restorative Dentistry 13,* 521-529, (1993).

[11] Lang, N.P. and Corbet, E.F., Diagnostic procedures in daily practive. *Int. Dental J. 45,* 5-15, (1995).

[12] Greenstein, G. and Lamster, I., Understanding diagnostic testing for periodontal diseases. *J. Periodontology 66,* 659-666, (1995).
[13] Listgarten, M.A., Periodontal probing: What does it mean? *J. Clin Periodontology 7,* 165, (1980).
[14] Trovato, J.P., The role of the general dentist in periodontal care. *General Dentistry* 176-181, March-April (2003).
[15] Tupta-Veselicky, L., Famili, P., Ceravolo, F.J. and Zullo, T., A clinical study of an electronic constant force periodontal probe. *J. Periodontoloy 65,* 616-622, (1994).
[16] Palou, M.E., McQuade, M.J. and Rossman, J.A.. The use of ultrasound for the determination of periodontal bone morphology. *J. Periodontology 58,* 262-265, (1987).
[17] Hunter, F., Periodontal probes and probing. *Int. Dental J. 44,* 557-583, (1994).
[18] Mayfield, L., Bratthall, G. and Attstrom, R., Periodontal probe precision using 4 different periodontal probes. *J. Clin. Periodontology 23,* 76-82, (1996).
[19] Jeffcoat, M.K., Machines in periodontics. *Scientific 84,* 18-22, (1991).
[20] Quiryen, M., Callens, A., Steenberghe, D.V., and Nys, M., Clinical evaluation of a constant force electronic probe. *J. Periodontology 64,* 35-39, (1993).
[21] Cattabriga, M., Future diagnostic possibilities in periodontology. *Int. Dental J. 43,* 109-115, (1993).
[22] Grossl, S.G., Dunford, R.G., Koch, H.A., Machtei, E.E., Genco, R.J., Sources of error in periodontal probing measurements. *J. Periodontal Research 31,* 330-336, (1996).
[23] Barendregt, D.S., Velden, U. van der, Relker, J. and Loos, B.G.. Clinical evaluation of tine shape of 3 periodontal probes using 2 probing forces. *J. Clin. Periodontology 23,* 397-402, (1996).
[24] Garnick, J.J. and Silverstein, L.. Periodontal probing: probe tip diameter. *J. Periodontology 71,* 96-103, (2000).
[25] Wang, S.F., et al. Reproducibility of periodontal probing using a conventional manual and an automated force-controlled electronic probe. *J. Periodontology 66,* 38-46, (1995).
[26] Tessier, J.F., et al. Relationship between periodontal probing velocity and gingival inflammation in human subjects. *J. Clin. Periodontology 20,* 41-48, (1993).
[27] Tupta-Veselicky, L., et al. A clinical study of an electronic constant force periodontal probe. *J. Periodontology 65,* 616-622, (1994).
[28] Cattabriga, M., Future diagnostic possibilities in periodontology. *Int. Dental J. 43,* 109-115, (1993).
[29] Yang, M.C.K., et al. Reproducibility of an electronic probe in relative attachment level measurements. *J. Clin. Periodonoloty 19,* 306-311, (1992).
[30] Ahmed, N., Watts, T.L.P., and Wilson, R.F., An investigation of the validity of attachment level measurements with an automated periodontal probe. *J. Clin. Periodontology 23,* 452-455, (1996).
[31] Aguero, A., et al. Histological location of a standardized periodontal probe in man. *J. Periodontology 66,* 184-190, (1995).
[32] Keagle, J.G., et al. Effect of gingival wall on resistance to probing forces. *J. Clin. Periodontology 22,* 953-957, (1995).
[33] Fukukita, H., et al. Development and application of an ultrasonic imaging system for dental diagnosis. *J. Clin. Ultrasound 13,* 597-600, (1985).
[34] Lost, C., Irion, K.M., and Nussle, W., Periodontal ultrasonic diagnosis: experiments on thin bony platelets and on a simulated periodontal ligament space. *J. Periodontal Res 23,* 347-351, (1988).
[35] Palou, M.E., McQuade, M.J., and Rossman, J.A., The use of ultrasound for the determination of periodontal bone morphology. *J. Periodontology 58,* 262-265, (1986).
[36] Ng, S.K., Songra, A., Ali, N. and Carter, J.L.B.. Ultrasound features of osteosarcoma of the mandible—a first report. *Oral Surgery Oral Medicine Pathology, 92,* #5, 582-586 (2001).
[37] Hamano, N., Hanaoka, K., Ebihara, K., Toyada, M. and Teranaka, T., Evaluation of Adhesive Defects using an Ultrasonic Pulse-reflection Technique. *Dental Materials Journal, 22* #1, 66-79 (2003).

[38] Ghorayeb, S.R. and Valle T., Experimental Evaluation of Human Teeth Using Noninvasive Ultrasound: Echodentography. *IEEE Transactions on Ultrasonics, Ferroelectrics, and Frequency Control 49,* 1437-1443 (2002).

[39] Tsiolis, F.I, I.G. Needleman and G.S. Griffiths, Periodontal ultrasononography. *J. Clinical Periodontology 30*, 849-854 (2003).

[40] Lassal, A.C. and Payne, P.A., Scanning and imaging using lamb waves. *Acoustical Imaging 23,* 355-61, (1997).

[41] Companion, J.A., Differential Measurement Periodontal Structures Mapping System, US Patent #5,755,571 (1998).

[42] Loker, D.R. and Hagenbuch K., Ultrasonic periodontal diagnostic instrumentation system with clinical results. *Measurement 23,* 125-129, (1998).

[43] Hinders, M.K. and Companion J., "Ultrasonic periodontal probe," In D.E. Chimenti and D.O. Thompson, editors, *Review of Progress in Quantitative Nondestructive Evaluation 18,* 1609-1615. Kluwer Academic/Plenum Publishers, 1999.

[44] Lynch, J.E., "Development and clinical testing of an ultrasonographic periodontal probe." [Dissertation]. Williamsburg, Virginia: College of William and Mary; 2001.

[45] Hinders, M.K., Lynch, J.E., and McCombs, G., "Periodontal Disease Diagnosis using an Ultrasonic Probe," *Review of Progress in Quantitative Nondestructive Evaluation, 21,* 1880-1887. D.O. Thompson and D.E. Chimenti, American Institute of Physics (2002).

[46] Lynch, J.E. and Hinders, M.K., Ultrasonic device for measuring periodontal attachment levels, *Review of Scientific Instruments 73,* No.7, 2686-2693, (2002).

[47] Rosiene, J. and Sholl, H., Application of wavelets to ultrasonic evaluation of thickness, *SPIE Wavelet Applications 2242*, 488-498, (1994).

[48] Abbate, A., Koay, J., Frankel, J., Schroeder, S.C. and Das, P., Application of wavelet transform signal processor to ultrasound, in *IEEE Ultrasonic Symposium Proceedings*, pp.1147-1152, (1994).

[49] Strickland R.N. and Hahn H., Wavelet transforms for detecting microcalcifications in mammograms, *IEEE Transactions on Medical Imaging 15,* 218-229, (1996).

[50] Xu, X.L., Tewfik, A.H. and Greenleaf, J.F., Time delay estimation using wavelet transform for pulsed-wave ultrasound, *Annals of Biomedical Engineering 23*, 612-621, (1995).

[51] Xu, X.L. and Greenleaf, J.F., Wavelet transform for cross correlation processing in PW ultrasound, in *Proceedings of the 16th Annual International Conference of the IEEE Engineering in Medicine and Biology Society*, 1224-1225, (1994).

[52] Georgiou, G. and Cohen, F.S., Tissue characterization using the continuous wavelet transform, *IEEE Transactions on Ultrasonics, Ferroelectrics, and Frequency Control 48,* 355-373, (2001).

[53] Szczuka, M. and Wojdyllo, P., Neuro-wavelet classifiers for EEG signals based on rough set methods, *Neurocomputing 36,* 103-22, (2001).

[54] Dokur Z. and Olmez T., ECG beat classification by a novel hybrid neural network, *Computer Methods & Programs in Biomedicine, 66,* 167-81, (2001).

[55] Legendre, S., Massicotte, D., Goyette, J. and Bose T.K., Neural classification of lamb wave ultrasonic weld testing signals using wavelet coefficients, *IEEE Transactions on Instrumentation and Measurement 50,* 672-678, (2001).

[56] Lemistre, M. and Balageas, D., Structural health monitoring system based on diffracted Lamb wave analysis by multi-resolution procession, *Smart Materials and Structures 10*, 504-511, (2001).

[57] Hou, J.D. and Hinders, M.K., Dynamic wavelet fingerprint identification of ultrasound signals, *Materials Evaluation 60,* 1089-1093, (2002).

[58] Abbate, A., Koay, J., Frankel, J., Schroeder, S.C. and Das, P., Signal detection and noise suppression using a wavelet transform signal processor: application to ultrasonic flaw detection, *IEEE Transaction on Ultrasonics, Ferroelectrics, and Frequency Control 44,* 14-26, (1997).

[59] Coifman, R.R. and Donoho, D.L., Translation invariant de-noising, *Lecture Notes in Statistics 103,* 125-150, (1995).
[60] Daubechies, I., *Ten lectures on wavelets,* (Society for Industrial and Applied Mathematics, 1992).
[61] *Wavelet Toolbox: User's Guide.* (The MathWorks Inc. 2000).
[62] Bland, J.M. and Altman, D.G., Statistical methods for assessing agreement between two methods of clinical measurement, *Lancet 8476*, 307-310, (1986).